Journal of Computational Physics **165,** 752–770 (2000)
doi:10.1006/jcph.2000.6639, available online at http://www.idealibrary.com on IDEAL®

SPH Simulation of River Ice Dynamics

Hung Tao Shen, Junshan Su, and Lianwu Liu

Department of Civil and Environmental Engineering, Clarkson University, Potsdam, New York 13699-5710
E-mail: htshen@clarkson.edu

Received March 15, 2000; revised September 27, 2000

This paper describes a two-dimensional numerical model for dynamic transport and jamming of surface ice in rivers. The hydrodynamic component of the model uses an Eulerian finite-element method, while the ice dynamic component uses the smoothed particle hydrodynamics method. The model considers the moving surface ice as a continuum. The internal ice resistance is formulated with a viscous–plastic constitutive law, in which the pressure term is formulated by modifying the Coulomb-type constitutive relationship for static ice jams. The partial-slip boundary condition for ice along solid boundaries is treated by the method of images. The model is verified with an analytical solution and used to examine the feasibility of using ice booms to reduce the jamming potential in the Mississippi–Missouri River confluence.

Key Words: SPH method; ice dynamics; river ice; ice jams; Lagrangian method; particle method.

1. INTRODUCTION

Surface ice runs and ice jams are important river ice processes. Ice runs and ice jams can interfere with inland navigation, damage hydraulic structures, and cause excessive shoreline erosion. Ice jams can also cause severe flooding by reducing the flow cross section and increasing the flow resistance. The ice jam theory based on static equilibrium of floating accumulations of granular ice is well developed [3]. Flato and Gerard [8] and Beltaos [2] developed one-dimensional numerical models for computing static ice jam profiles. Since the dynamics of ice motion were not considered, the static ice jam theory could not be used to determine whether, when, and where a jam would form. Moreover, the momentum effects of ice and water flows on ice jam evolution and thickness were not accounted for in the static ice jam theories. Shen *et al.* [38] developed an analytical framework for the dynamic transport of river ice and ice jam formation. Lal and Shen [18] developed a one-dimensional numerical model using the MacCormack method [23] to simulate the river ice transport. They examined the characteristics of the coupled ice dynamic and hydrodynamic equations and showed that the leading edge of an ice jam acts as a shock front for the stress wave in the

0021-9991/00 $35.00

ice layer. They also showed that the speed of the shallow water wave is not affected by the ice condition and that the speed of the stress wave in the ice layer is not related to shallow water wave characteristics. As a result of this independence, water and ice flow equations need not be solved simultaneously. One-dimensional models have limited applicability, since river ice transport and jam processes are two-dimensional phenomena owing to the existence of bank friction, irregular channel geometry, and non-uniform water current.

The basic concept of river ice transport is similar to those of sea ice transport [16] and lake ice transport [41]. However, river ice transport is a more dynamic phenomenon. River ice problems have much smaller temporal and spatial scales than lake and sea ice problems and generally have much larger convective terms and larger variations in velocity and concentration. Most of the existing numerical models for sea ice and lake ice dynamics are based on Eulerian finite-difference methods, which have large numerical diffusion and dispersion [16, 41]. Pritchard *et al.* [33] introduced an adaptive grid scheme, which uses Lagrangian grid cells to follow the motion of the ice edge and reduce the numerical diffusion across the ice edge. However, this method does not improve the accuracy of the simulation inside the ice field. Moreover, the method will break down when large ice edge displacement leads to the rapid distortion of grid cells. Flato [7] applied the particle-in-cell (PIC) method [13] to the sea ice problem. Although the PIC method is more versatile than the Lagrangian adaptive grid scheme, it still suffers large numerical diffusion due to the back and forth interpolations between grids and particles at each time step.

The pure Lagrangian method of smoothed particle hydrodynamics (SPH) introduced by Lucy [22] and Gingold and Monaghan [9, 10] avoids the particle–grid interpolations. The method was originally developed for astrophysical fluid dynamics [11, 15, 26, 28, 34] and cosmological gas dynamics [6]. Most of these early applications were developed for problems in infinite domains for media of homogeneous material properties subject to gravity force only [4]. More recently, the method has been applied to a wider range of flow problems [28]. Shen *et al.* [37] applied SPH to simulate the two-dimensional dynamic transport of river ice. This was the first application of SPH to ice dynamics, which involves the full stress tensor with varying material properties.

In the present study, the model of Shen *et al.* [37] is refined by including the water discharge in the ice layer in the hydrodynamic equations. A nonlinear seepage theory is used to simulate the gradient-induced water flow in the ice layer. With these modifications, the flow in a grounded ice jam can be correctly modeled and the water mass is conserved. The Lagrangian model for ice transport is also refined.

2. GOVERNING EQUATIONS

The movement of surface ice runs in a river is governed by current and wind drag, gravity, interaction between ice elements, and their interactions with river boundaries and hydraulic structures.

2.1. *Ice Dynamic Equations*

Considering the surface ice layer in the river as a continuum, the momentum equation can be written in a Lagrangian form as

$$M\frac{D\mathbf{V}}{Dt} = \mathbf{R} + \mathbf{F}_a + \mathbf{F}_w + \mathbf{G}, \tag{1}$$

in which $\mathbf{V} = u\mathbf{i} + v\mathbf{j}$, ice velocity; $\frac{D}{Dt} = \frac{\partial}{\partial t} + u\frac{\partial}{\partial x} + v\frac{\partial}{\partial y}$; $\frac{D\mathbf{V}}{Dt}$ is acceleration of ice mass; $M = \rho_i N t_i$ is ice mass per unit area, i.e., the two-dimensional ice mass density; x, y, and t are space and time variables; ρ_i, N, t_i are density, area concentration, and thickness of ice, respectively; $\mathbf{R} = \mathbf{i}[\frac{\partial}{\partial x}(\sigma_{xx} N t_i) + \frac{\partial}{\partial y}(\sigma_{xy} N t_i)] + \mathbf{j}[\frac{\partial}{\partial x}(\sigma_{yx} N t_i) + \frac{\partial}{\partial y}(\sigma_{yy} N t_i)]$, internal ice resistance; σ_{xx}, σ_{yy} are normal stress components; $\sigma_{xy} = \sigma_{yx}$ are shear stress components; $\mathbf{F}_a = N\rho_a c_a |\mathbf{W}|\mathbf{W}$, wind drag at the air–ice interface; $\mathbf{W} = \mathbf{i}W_x + \mathbf{j}W_y$, surface wind velocity at 10 m above the water surface; ρ_a is the density of air; c_a is the wind drag coefficient; $\mathbf{F}_w = N\rho c_w |\mathbf{V}_w - \mathbf{V}|(\mathbf{V}_w - \mathbf{V})$, water drag at the ice–water interface; $\mathbf{V}_w$ is depth-averaged current velocity; ρ is water density; c_w is the water drag coefficient, which is a function of the ice roughness and ice and current velocities [36, 38]; $\mathbf{G}$ is gravitational force due to the water surface slope, $-Mg\nabla\eta$; and η is the water surface elevation.

The ice mass conservation equation is

$$\frac{DM}{Dt} + M\nabla \cdot \mathbf{V} = 0. \tag{2}$$

Since the ice mass per unit area, M, is determined by the ice concentration, N, and ice layer thickness, t_i, one more conservation equation is needed. The equation of conservation of ice area within an elemental control area can be obtained by considering the ice area flux into and out of the control area and the ice area change due to mechanical redistribution,

$$\frac{DN}{Dt} + N\nabla \cdot \mathbf{V} + R_a = 0, \tag{3}$$

in which R_a is the rate of change of ice area due to mechanical redistribution. Equations (2) and (3) can be combined to yield an ice thickness conservation equation:

$$\frac{\partial t_i}{\partial t} = -\mathbf{V} \cdot \nabla t_i + \frac{t_i}{N} R_a. \tag{4}$$

A constitutive law is required to describe the ice internal stress. In this study, the widely used viscous–plastic law [16, 41] is adopted,

$$\sigma_{ij} = 2\upsilon\dot{\varepsilon}_{ij} + (\varsigma - \upsilon)\dot{\varepsilon}_k\delta_{ij} - P\delta_{ij}/2, \tag{5}$$

in which ς, υ, nonlinear bulk and shear viscosity, are defined as

$$\varsigma = \frac{P}{2\Delta} \qquad \text{and} \qquad \upsilon = \frac{\varsigma}{e^2}, \tag{6}$$

in which $\Delta^2 = D_I^2 + (D_{II}/e)^2$; $D_I D_{II}$ are the first and second invariant strain rates, respectively; $D_I = \dot{\varepsilon}_{xx} + \dot{\varepsilon}_{yy}$; $D_{II} = [(\dot{\varepsilon}_{xx} - \dot{\varepsilon}_{yy})^2 + 4\dot{\varepsilon}_{xy}^2]^{1/2}$; $e = 2$, the principal axes ratio of the elliptical yield curve; $\dot{\varepsilon}_{xx} = \partial u/\partial x$; $\dot{\varepsilon}_{yy} = \partial v/\partial y$; and $\dot{\varepsilon}_{xy} = \frac{1}{2}(\frac{\partial v}{\partial x} + \frac{\partial u}{\partial y})$. Shen *et al.* [38] suggested an expression for the pressure term, by extending the constitutive relationship for static ice jams, as

$$P = \tan^2\left(\frac{\pi}{4} + \frac{\phi}{2}\right)\left(1 - \frac{\rho_i}{\rho}\right)\frac{\rho_i g t_i}{2}\left(\frac{N}{N_{\max}}\right)^j \tag{7}$$

in which ϕ is the internal friction angle of ice, 46°; $N_{\max}$ is the maximum allowable ice concentration, 0.6; and $j = 15$, an empirical constant.

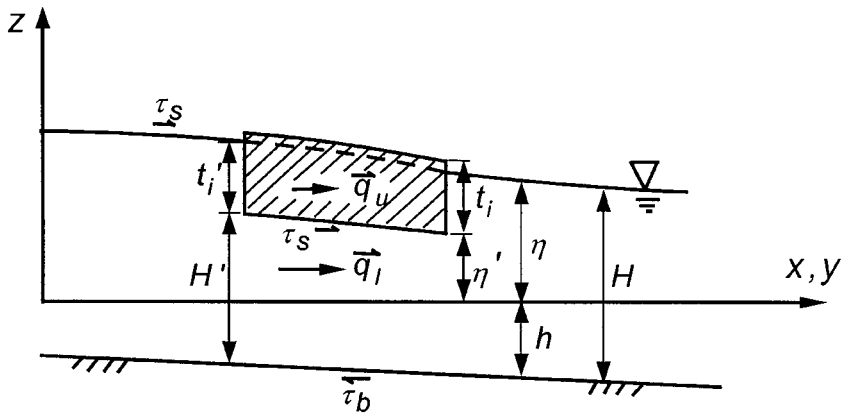

FIG. 1. Definition sketch.

2.2. *Hydrodynamic Equations*

Figure 1 shows a definition sketch of river flow with a layer of moving surface-ice floes. The river water discharge is divided into two parts: the discharge in the upper layer, or the ice layer, and the discharge in the lower layer, or the water layer.

The water in the ice layer moves with the ice, but is modified by the relative flow produced by the water surface gradient. The unit width discharge in the ice layer can be written as

$$\mathbf{q}_u = \mathbf{V}\Delta H(1-N) + \mathbf{q}_s = \mathbf{q}_i + \mathbf{q}_s, \tag{8}$$

in which $\mathbf{q}_i$ is the flow carried by the moving ice; $\mathbf{q}_s = \mathbf{V}_s \Delta H$; $\mathbf{V}_s = u_s\mathbf{i} + v_s\mathbf{j}$, the apparent seepage velocity in the ice layer produced by the hydraulic gradient $\mathbf{j} = (\frac{\partial \eta}{\partial x}\mathbf{i} + \frac{\partial \eta}{\partial y}\mathbf{j})$; $N =$ ice concentration; and $\delta H = H - H'$, submerged ice layer thickness. The velocity $\mathbf{V}_s$ is related to the surface gradient J by the Ergun formula [1],

$$V_s = \lambda\sqrt{J}, \tag{9}$$

in which the seepage coefficient λ is related to the porosity, shape, and size of the ice floes. Field data indicate that this coefficient has an average value of about 1.6 m/s for breakup jams [2, 3].

The conservation of water and ice mass gives the continuity equation

$$\frac{\partial}{\partial t}[\rho H' + \rho(1-N)t_i' + \rho_i t_i N] = \nabla \cdot (\rho \mathbf{q}_l + \rho \mathbf{q}_u + \rho_i \mathbf{q}_{ice}), \tag{10}$$

where $t_i' = \rho_i t_i/\rho$ is the submerged ice thickness; ρ is water density; $H' = \eta' + h$, water depth beneath the ice layer; h is water depth below the reference level; $\mathbf{q}_l$ is unit-width discharge in the lower layer; and $\mathbf{q}_{ice}$ is unit-width ice discharge. For a floating surface ice layer, $H' = H - t_i'$; i.e., $\Delta H = t_i'$. When (10) is combined with the ice mass conservation equation, the continuity equation for water flow becomes

$$\frac{\partial H}{\partial t} + \nabla \cdot (\mathbf{q}_l + \mathbf{q}_i + \mathbf{q}_s) = \frac{\partial}{\partial t}(N t_i'). \tag{11}$$

When the ice is grounded, regardless of whether it is moving or stationary, the condition $\Delta H = t_i'$ is no longer valid, and $\mathbf{q}_l$ is zero. In this case, as shown in Fig. 2, the conservation

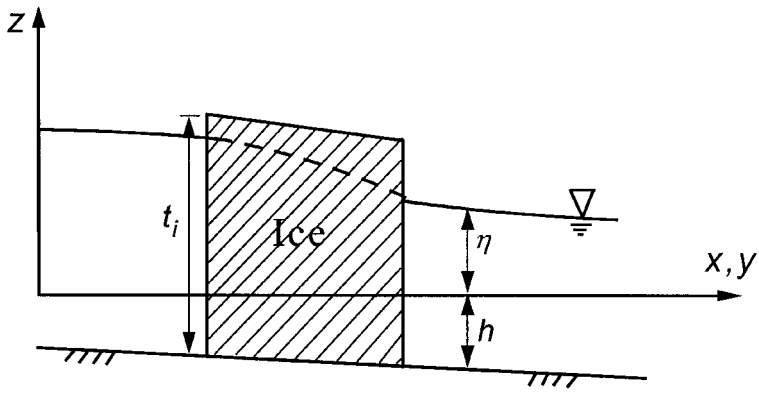

FIG. 2. Definition sketch for a grounded ice accumulation.

of water mass becomes

$$\frac{\partial}{\partial t}[(1-N)\Delta H] + \nabla \cdot (\mathbf{q}_{\mathrm{i}} + \mathbf{q}_{\mathrm{s}}) = 0 \tag{12}$$

or

$$\frac{\partial H}{\partial t} + \nabla \cdot (\mathbf{q}_{\mathrm{i}} + \mathbf{q}_{\mathrm{s}}) = \frac{\partial}{\partial t}(NH). \tag{13}$$

Neglecting the momentum exchange across the interface between the ice and water layers, the momentum equations can be written as

$$\frac{\partial q_{\mathrm{l}x}}{\partial t} + \frac{\partial}{\partial x}\left(\frac{q_{\mathrm{l}x}^2}{H'}\right) + \frac{\partial}{\partial y}\left(\frac{q_{\mathrm{l}x} q_{\mathrm{l}y}}{H'}\right) = -gH'\frac{\partial \eta}{\partial x} + \frac{1}{\rho}(\tau_{\mathrm{b}x} - \tau_{\mathrm{s}x}) + \frac{1}{\rho}\frac{\partial T_{xx}}{\partial x} + \frac{1}{\rho}\frac{\partial T_{xy}}{\partial y} \tag{14}$$

and

$$\frac{\partial q_{\mathrm{l}y}}{\partial t} + \frac{\partial}{\partial y}\left(\frac{q_{\mathrm{l}y}^2}{H'}\right) + \frac{\partial}{\partial x}\left(\frac{q_{\mathrm{l}x} q_{\mathrm{l}y}}{H'}\right) = -gH'\frac{\partial \eta}{\partial y} + \frac{1}{\rho}(\tau_{\mathrm{b}y} - \tau_{\mathrm{s}y}) + \frac{1}{\rho}\frac{\partial T_{yy}}{\partial y} + \frac{1}{\rho}\frac{\partial T_{yx}}{\partial x}, \tag{15}$$

in which $\boldsymbol{\tau}_{\mathrm{s}}$, $\boldsymbol{\tau}_{\mathrm{b}}$ are shear stresses at the ice–water interface and on the river bed, respectively; $T_{jk} = \varepsilon_{jk}^{w}(\frac{\partial q_{\mathrm{l}j}}{\partial x_k} + \frac{q_{\mathrm{l}k}}{\partial x_j})$, where j and k denote x and y coordinate directions; and ε_{jk}^{w} is the generalized eddy viscosity coefficient.

3. MODEL IMPLEMENTATION

A finite element model using the lumped mass technique and leapfrog time integration [5] is used for the hydrodynamic component. The ice dynamic simulation using SPH is presented here. The ice dynamic and hydrodynamic components are coupled through the interaction at the interface between the two layers.

3.1. *SPH Simulation*

The ice dynamic equations are solved using the SPH method [25, 26]. The movement of ice is simulated with a sufficiently large number of particles, which carry mass, momentum,

and energy. The term *particle* represents a material element, which is an ice parcel containing a collection of ice pieces. The non-advective terms in the equations are simulated by interpolating the property of the tracing particle with its neighboring particles. We define m_j and M_j as the mass and mass density of particle j located at $\mathbf{r}_j$, and n_j as the number density, i.e., number of particles per unit area. By considering that $M_j = n_j m_j$, the kernel estimation of a function $f(\mathbf{r})$ can be expressed as [26]

$$\tilde{f}(\mathbf{r}, l) = \sum_{j=1}^{N} \frac{f_j}{n_j} W(\mathbf{r} - \mathbf{r}_j, l) = \sum_{j=1}^{N} f_j \frac{m_j}{M_j} W(\mathbf{r} - \mathbf{r}_j, l), \tag{16}$$

in which l is the smoothing length, which determines the range of influence of the interpolation kernel W. In the present study, the following Gaussian kernel is used:

$$G(\mathbf{r}, \mathbf{r}_j, l) = \frac{1}{\pi l^2} e^{-(\mathbf{r}-\mathbf{r}_j)^2/l^2}. \tag{17}$$

The mass density at the location of parcel k, $\mathbf{r}_k$, can be obtained from Eq. (16) as

$$M_k = \sum_j m_j W(\mathbf{r}_k - \mathbf{r}_j, l) = \sum_j m_j W_{kj}, \tag{18}$$

in which W_{kj} denotes the average of interpolation kernels of parcel k and j, $W_{kj} = [W(\mathbf{r}_{kj}, l_k) + W(\mathbf{r}_{kj}, l_j)]/2$ [15]. The ice mass is automatically conserved in the above form. The ice concentration can be determined from the calculated ice mass density. The ice area concentration is first calculated from the single layer ice thickness t_{i_o}; i.e., $N_k = M_k/(\rho_i t_{i_o})$. The ice concentration is limited by its maximum value $N_{\max}$. When this limit is reached mechanical thickening occurs. Since $M_k = \rho_i N_k t_{i_o} = \rho_i N_{\max}(t_i)_k$, the ice thickness is modified to $(t_i)_k = M_k/(\rho_i N_{\max})$.

The momentum balance of particle k gives its acceleration,

$$\mathbf{a}_k = \left(\frac{D\mathbf{V}}{Dt}\right)_k = \frac{1}{M_k}[\mathbf{R}_k + (\mathbf{F}_a)_k + (\mathbf{F}_w)_k + \mathbf{G}_k]. \tag{19}$$

The internal and external forces can be calculated as the following [36]:

- Internal ice resistance $(\mathbf{R})_k = \mathbf{i}(R_x)_k + \mathbf{j}(R_y)_k$,

$$\frac{1}{(M_i)_k}(R_x)_k = \sum_j m_j \left\{ \left[\frac{(\sigma_{xx} N t_i)_k}{(M_i)_k^2} + \frac{(\sigma_{xx} N t_i)_j}{(M_i)_j^2} \right] \frac{\partial W_{kj}}{\partial x} + \left[\frac{(\sigma_{xy} N t_i)_k}{(M_i)_k^2} + \frac{(\sigma_{xy} N t_i)_j}{(M_i)_j^2} \right] \frac{\partial W_{kj}}{\partial y} \right\}, \tag{20}$$

$$\frac{1}{(M_i)_k}(R_y)_k = \sum_j m_j \left\{ \left[\frac{(\sigma_{yy} N t_i)_k}{(M_i)_k^2} + \frac{(\sigma_{yy} N t_i)_j}{(M_i)_j^2} \right] \frac{\partial W_{kj}}{\partial y} + \left[\frac{(\sigma_{yx} N t_i)_k}{(M_i)_k^2} + \frac{(\sigma_{yx} N t_i)_j}{(M_i)_j^2} \right] \frac{\partial W_{kj}}{\partial x} \right\}, \tag{21}$$

in which $(\sigma_{xx})_k$, $(\sigma_{yy})_k$, and $(\sigma_{xy})_k = (\sigma_{yx})_k$ are internal stresses at $\mathbf{r}_k$, where parcel k is located. From the viscous constitutive law they can be expressed in terms of velocity

gradients, viscosity coefficients, and ice pressure as

$$(\sigma_{xx})_k = 2\upsilon_k\left(\frac{\partial u}{\partial y}\right)_k - (\varsigma_k - \upsilon_k)\left[\left(\frac{\partial u}{\partial x}\right)_k + \left(\frac{\partial v}{\partial y}\right)_k\right] - \frac{P_k}{2} \tag{22}$$

$$(\sigma_{yy})_k = 2\upsilon_k\left(\frac{\partial v}{\partial y}\right)_k - (\varsigma_k - \upsilon_k)\left[\left(\frac{\partial u}{\partial x}\right)_k + \left(\frac{\partial v}{\partial y}\right)_k\right] - \frac{P_k}{2} \tag{23}$$

$$(\sigma_{xy})_k = \upsilon_k\left[\left(\frac{\partial v}{\partial y}\right)_k + \left(\frac{\partial u}{\partial x}\right)_k\right]. \tag{24}$$

The velocity gradients can be expressed as

$$\left(\frac{\partial u}{\partial x}\right)_k = \frac{1}{(M_i)_k}\sum_j m_j(u_j - u_k)\frac{\partial W_{kj}}{\partial x} \tag{25}$$

$$\left(\frac{\partial u}{\partial y}\right)_k = \frac{1}{(M_i)_k}\sum_j m_j(u_j - u_k)\frac{\partial W_{kj}}{\partial y} \tag{26}$$

$$\left(\frac{\partial v}{\partial x}\right)_k = \frac{1}{(M_i)_k}\sum_j m_j(v_j - v_k)\frac{\partial W_{kj}}{\partial x} \tag{27}$$

$$\left(\frac{\partial v}{\partial y}\right)_k = \frac{1}{(M_i)_k}\sum_j m_j(v_j - v_k)\frac{\partial W_{kj}}{\partial y}. \tag{28}$$

- Wind drag $(\mathbf{F}_a)_k = \mathbf{i}(\tau_{ax}N)_k + \mathbf{j}(\tau_{ay}N)_k$,

$$(\tau_{ax})_k = \rho_a c_a |\mathbf{W}|_k (W_x)_k \tag{29}$$

$$(\tau_{ay})_k = \rho_a c_a |\mathbf{W}|_k (W_y)_k, \tag{30}$$

in which $(\mathbf{W})_k$ is the wind velocity at the location of parcel k.

- Water drag $(\mathbf{F}_w)_k = \mathbf{i}(\tau_{wx}N)_k + \mathbf{j}(\tau_{wy}N)_k$,

$$(\tau_{wx})_k = \rho c_w |\mathbf{V}_w - \mathbf{V}_i|_k (V_{wx} - u)_k \tag{31}$$

$$(\tau_{wy})_k = \rho c_w |\mathbf{V}_w - \mathbf{V}_i|_k (V_{wy} - v)_k, \tag{32}$$

in which $(\mathbf{V}_w)_k$ is the water current velocity at $\mathbf{r}_k$, and u_k, v_k are components of ice velocity of parcel k in x and y directions.

- Gravitational force $(\mathbf{G})_k = \mathbf{i}(G_x)_k + \mathbf{j}(G_y)_k$,

$$(G_x)_k = -(M_i)_k g\left(\frac{\partial \eta}{\partial x}\right)_k \tag{33}$$

$$(G_x)_k = -(M_i)_k g\left(\frac{\partial \eta}{\partial x}\right)_k. \tag{34}$$

Since the water drag force is a function of the square of ice velocity, it is difficult to integrate Eq. (19) explicitly. The fourth-order Runge–Kutta method is used to calculate the ice velocity at time t^{n+1}.

The leapfrog scheme for time stepping is applied. The parcel velocities are calculated at half time steps, i.e., $t^{n-1/2}$, $t^{n+1/2}$, ... Parcel positions are calculated at time t^n, t^{n+1}, ... The advance of the position of parcel k is calculated by

$$\mathbf{r}_k^{n+1} = \mathbf{r}_k^n + \Delta t \mathbf{V}_{ik}^*, \tag{35}$$

in which $\mathbf{V}_{ik}^* = \frac{1}{2}(\mathbf{V}_{ik}^{n-1/2} + \mathbf{V}_{ik}^{n+1/2})$. After all parcels move to their new positions, the distribution of ice properties such as mass density, concentration, and thickness can be updated by interpolations. For the leapfrog scheme, the stability condition or time step is limited by the Courant condition. The time step for parcel k is determined by

$$\delta t_k = \beta \min\left(\sqrt{\frac{l_k}{|a_k|}}, \frac{l_k}{|v_k| + c_k}\right), \tag{36}$$

where a_k and c_k are the parcel acceleration and speed of sound determined by the ice properties; β is the Courant number, which is 1.0.

Due to the small numerical diffusion, the SPH method often needs an artificial viscosity [4, 27, 31], especially for non-viscous material. The artificial viscosity mimics a bulk viscosity, which is used in the SPH method to damp the shock wave caused by the pressure term. The experience from the present study indicates that the artificial viscosity is not necessary for river ice dynamics because the ice viscosity and the water drag provide the necessary damping. The stability analysis of the SPH algorithm by Swegle *et al.* [39] showed that the instability would normally only occur in tension. It is not a problem in the present study. This is due to the negligible tensile stress in ice and the influence of the water drag on the ice motion.

3.2. *Bed Resistance*

The bed friction affects the motion of ice when it is grounded. The magnitude of the bed friction can be calculated from the submerged weight of the ice as

$$|\mathbf{F}_G| = N[\rho_i t_i - \rho(\eta + h)]g \tan\phi_b, \tag{37}$$

in which $\tan\phi_b$ the bed-to-ice friction coefficient. In the model, the bed frictional force always opposes the motion of the ice or its tendency to move. A local coordinate system is used for each parcel in calculating the parcel velocity. For an ice parcel having a velocity $\mathbf{V}^n \neq 0$ at t^n, the local x-coordinate is selected to coincide with the direction of $\mathbf{V}^n$. The x and y components of the equation of motion are

$$\frac{Du}{Dt} = F_{t,x}^n - |F_{G,x}| \tag{38}$$

and

$$\frac{Dv}{Dt} = \begin{cases} F_{t,y}^n - |F_{G,y}| & \text{if } F_{t,y}^n > F_{G,y} \\ 0 & \text{if } F_{t,y}^n \leq F_{G,y} \end{cases}, \tag{39}$$

in which F_t^n is the total force acting on the parcel, excluding the bed friction force. If $\mathbf{V}^n = 0$, then choose the local coordinate to coincide with the global coordinate, and both x and y components of the equation of motion are the same as Eq. (39).

3.3. *Boundary Conditions*

Upstream boundary conditions consist of ice concentration, thickness, and velocity. The free drift approximation may be used because the observed ice velocity at the boundary is usually not available. Along solid boundaries, such as riverbanks or dikes, the boundary resistance to the ice motion needs to be considered. The boundary friction exists only when the ice is moving toward the boundary. The boundary friction is calculated based on a dynamic Coulomb yield criterion [12],

$$F_f = F_c + F_N \tan \phi_B, \tag{40}$$

in which F_f is the friction force between the ice and the boundary; F_c is the cohesive force, assumed to be zero; $\tan \phi_B$ is the dynamic friction coefficient; and F_N is the normal component of the ice force acting on the boundary, which can be calculated from the component of internal ice force normal to the boundary, $R_N = \sigma_N N t_i l_B$. The contact length of the boundary ice parcel, l_B, can be approximated by the square root of the parcel area $\Delta A = m/(\rho_i N t_i)$. Similar to the bed resistance, the bank friction F_f always opposes the tangential motion, or the tendency of the motion, of the ice along the bank. To determine R_N, the interaction between the ice particle and the solid boundary has to be formulated. Several methods, including immobile boundary particle, repulsive forces, and the method of images, have been used in SPH to implement solid boundary conditions [24]. The immobile boundary particle method involves placing stationary particles of fixed size along the solid boundary. These particles are included in the summations, and their velocities are set to zero after each time step. Since the size and momentum of moving particles change with time, they may be pushed across the boundary due to the unbalanced ice force. This method is only valid for inactive boundaries where there are no new forces being applied to the boundary [24]. The repulsive force model [29, 30] has the same problem of particles crossing over as the immobile particle method, since the force coefficients are assumed to be constant. The method of images has been used by Libersky and Petschek [19] and Shen and Chen [36]. In this study, the partial-slip solid boundary condition will be implemented using the method of images. In this method, an imaginary particle is placed on the opposite side of the boundary for every real particle that is located within a normal distance $2l$ of the boundary. Each imaginary particle has the same mass, concentration, pressure, and tangential velocity as the corresponding real particle. The normal velocity is opposite that of the real particle; i.e., $v_n^* = -v_n$ and $v_t^* = v_t$, where v_t is tangential velocity, v_n is normal velocity, and the superscript $*$ denotes quantities associated with an imaginary particle. The normal internal stresses of imaginary parcels are the same as those of the real ones—i.e., $\sigma^*_{xx_j} = \sigma_{xx_j}$, $\sigma^*_{yy_j} = \sigma_{yy_j}$—but the shear stress is in the opposite direction—i.e., $\sigma^*_{xy_j} = -\sigma_{xy_j}$.

3.4. *Smoothing Length and Search Area*

Since the density of the particle distribution changes in space and time, it is necessary to vary the smoothing length of particles in order to achieve maximum efficiency and accuracy. Each particle should have its own smoothing length. Gingold and Monaghan [10] suggested that for two-dimensional problems, the smoothing length l should be inversely proportional to the square root of the particle number density. In the ice dynamics simulation, the smoothing length can be estimated as $l^{n+1} = l_0(\frac{M_0}{M^n})^{1/2}$, in which l_0 is the initial smoothing length, and M_0 is the initial mass density. In the model, l_0 is selected to be the

linear dimension of the initial parcel area, $\sqrt{\Delta A_0}$. Benz [4] developed an evolution equation for smoothing length as $\frac{dl}{dt} = \frac{1}{2} l \nabla \cdot \mathbf{V}$. Hence, the smoothing length is formulated as

$$l^{n+1} = l_*^{n+1} + \frac{\Delta t}{2} l_*^{n+1} (\nabla \cdot \mathbf{V})^n \tag{41}$$

and

$$l_*^{n+1} = l_0 \left(\frac{M_0}{M^n} \right)^{1/2}. \tag{42}$$

Theoretically, the larger the search range the higher the accuracy. However, the simulation time will increase dramatically with the search area, especially in a high-ice-concentration area where many particles accumulate in a small area. On the other hand, a small search area may cause stability problems [39]. Considering accuracy, stability, and simulation time, a suitable search range should be selected. The search area can be estimated by considering an ice field with uniformly distributed particles of the same mass m, size ΔA, and density M. Based on its definition, the particle mass is

$$m = \Delta A M = \Delta x \Delta y \rho_{\mathrm{i}} N t_{\mathrm{i}}, \tag{43}$$

where $\Delta x \Delta y = \Delta A$, parcel size. If the smoothing length is selected as

$$l = l_x = l_y = \Delta x = \Delta y, \tag{44}$$

then a square search area of $(4l \times 4l)$ centered at $\mathbf{r}_k$ will encompass 5×5 parcels. The mass density at $\mathbf{r}_k$ can be determined from Eq. (18) using the Gaussian kernel as

$$\begin{aligned} M_k &= \sum_j m_j W_{kj} = \sum_j \frac{\Delta A_j}{l^2 \pi} e^{-(r_k - r_j)^2 / l^2} \\ &= \frac{\Delta x \Delta y}{l^2 \pi} \left(1 + \frac{4}{e} + \frac{4}{e^4} + \frac{4}{e^2} + \frac{4}{e^8} + \frac{8}{e^5} \right) M_j \\ &= 0.999928 M. \end{aligned} \tag{45}$$

This shows that a search area of $4l \times 4l$ is sufficient if the smoothing length is $\sqrt{\Delta A}$.

3.5. *Search of Neighboring Particles*

The algorithm for particle search plays an important role in the SPH method. The linked-list method, which uses grid cells as a bookkeeping device, is the method most commonly used in particle simulation [17]. Although it is an efficient search method, an auxiliary grid system is required. Since the method is grid-based, asymmetrical searches and inaccuracies in interpolation may result when the reference particle is not located near the center of a grid. Another disadvantage of the method is that the search is performed grid by grid, which results in unnecessary searches, especially when the particle distribution is highly non-uniform in the search area. Rhoades [35] proposed an improved algorithm for SPH that is similar to the linked-list method. Although the method remains grid-based, the search is performed particle by particle, instead of grid by grid, to save computing time. The result

is a method slightly faster than the conventional linked-list method. Another advantage of the method is that the number of particles in each cell at the current time step is known. This can provide an estimate of the density and smoothing length. However, since the grid size cannot be changed during the simulation, the asymmetrical search problem remains. In addition, a three-dimensional array is required for two-dimensional simulations. Hernquist and Katz [15] suggested the use of the hierarchical tree algorithm, which does not require a grid. Although the search area is flexible, the method is time-intensive. The present study utilizes a sorted-list algorithm to search for neighboring particles. There are a number of sorted-list methods available, as reviewed by Helman *et al.* [14]. Considering that a river ice problem usually has a long narrow solution domain, the HeapSort method is used in the present model, with the x-coordinates of the particles as the heap key to permit a variable search area.

4. MODEL VERIFICATION

An analytical solution for the width-averaged static ice jam thickness profile can be obtained for an idealized ice jam. For a hypothetical straight uniform rectangular channel with uniform current and for which wind velocity, bank friction, and water surface slope are all assumed to be zero, only the x-component of the momentum equation needs to be considered. Equation (1) reduces to

$$R_x + F_{wx} = 0, \tag{46}$$

in which $R_x = \frac{\partial}{\partial x}(PN_{\max}t_i)$; $F_{wx} = \rho C_w V_{wx}^2$, drag at the ice–water interface; V_{wx} is the current velocity; and C_w is the drag coefficient. Based on Eq. (46), a simple analytical solution for the thickness profile of the static ice jam can be obtained,

$$t_i = \left(t_{io}^2 + \frac{2\rho C_w V_{wx}^2}{\tan^2(\pi/4 + \phi/2)(1 - \rho_i/\rho)\rho_i g} x_j \right)^{1/2}, \tag{47}$$

in which t_{io} is the single layer ice thickness and x_j is the distance from the leading edge of the jam, where $t_i = t_{io}$.

When the bank friction is considered, an analytical solution for the width-averaged static ice jam thickness profile can be obtained by extending the solution of Pariset and Hausser [32],

$$t_i = t_{eq}\left(1 - e^{-(2\mu_1/B)x_j}\right)^{1/2}, \tag{48}$$

where the equilibrium ice thickness t_{eq} is [32]

$$t_{eq} = \left(\frac{BNC_w V_{wx}^2}{g\mu_2(\rho_i/\rho(1 - \rho_i/\rho)} \right)^{1/2}, \tag{49}$$

in which $\mu_2 = N \tan\phi(1 + \sin\phi)$ and $\mu_1 = \tan\phi(1 - \sin\phi)$ [3]. For $\phi = 46^\circ$, $\mu_2 = 1.068$ and $\mu_1 = 0.29$. The above solution of Pariset and Hausser [32] assumed that the ice layer is a continuum. Therefore the minimum jam thickness is not limited by the single-layer thickness t_{io} as in Eq. (47).

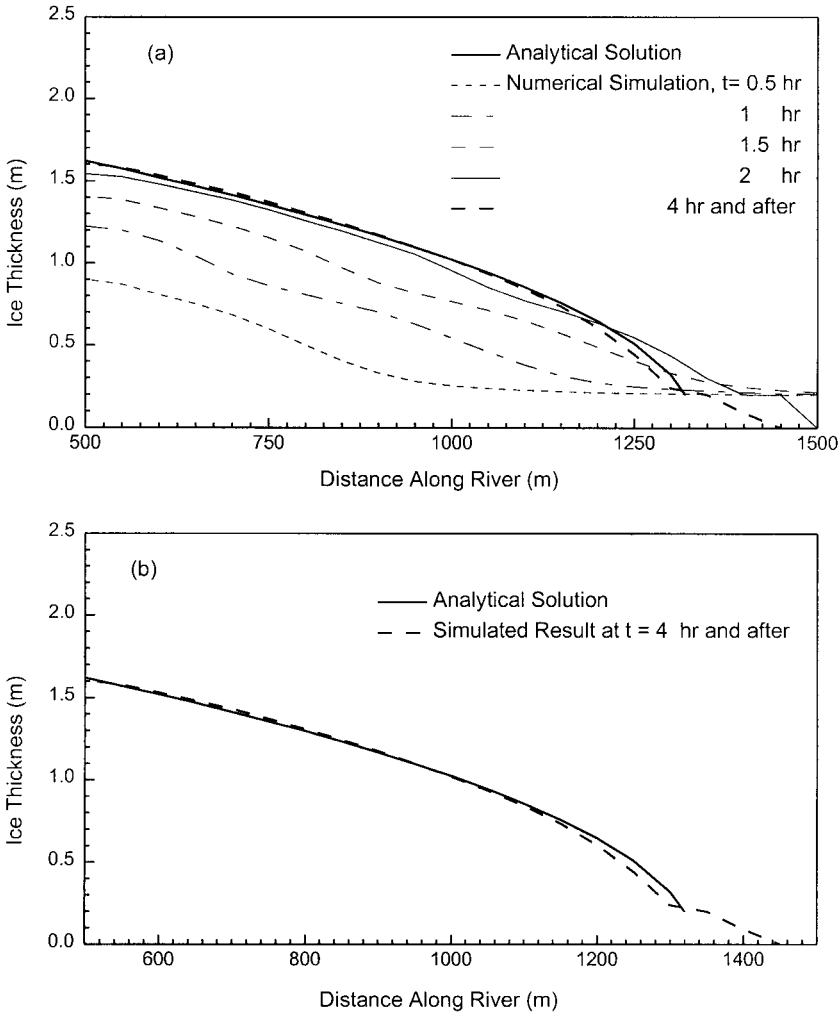

FIG. 3. Comparison of simulation results with the analytical solution, without bank resistance.

The numerical simulation results are compared in Figs. 3 and 4 with the analytical solutions. The channel has a length of 5000 m, a width of 500 m, a constant water velocity of 0.6 m/s, and a zero water-surface slope. The boom is located 500 m from the downstream boundary and assumed to be 100% effective; i.e., no ice is allowed to pass the boom. Initially, 900 ice parcels of size 50×50 m having a thickness of 0.2 m and a concentration of 0.6 are placed over the water surface between the upstream boundary and the boom. These ice floes are allowed to move toward the boom under the influence of the water drag. The coefficient C_w is 0.02. The analytical and numerical solutions give comparable results.

According to the viscous–plastic constitutive law, the viscosity approaches infinity when the ice approaches the static condition. A common way to avoid this singularity problem is to set a large limiting value for ς and υ in the numerical model. This approximation changes the constitutive relationship to a linear viscous law and the shear stress approaches zero when the strain rate approaches zero. Such a change will not be able to simulate the stoppage of ice motion and the jam formation. In this study, the constitutive law is modified for small strain rate conditions to avoid this problem. In the simulation, critical values of

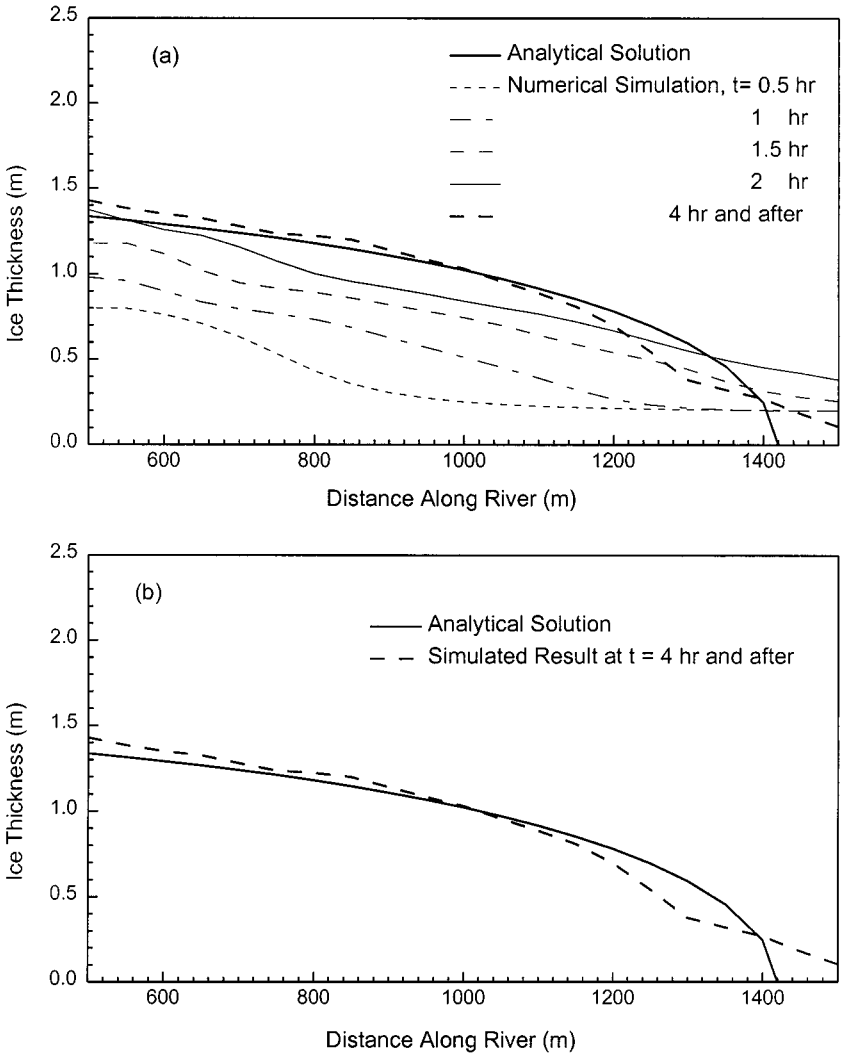

FIG. 4. Comparison of simulation results with the analytical solution, with bank resistance.

σ_{ij} and P for each ice parcel are determined when the following conditions are satisfied: (1) ice parcel velocity is less than a small critical value (0.001 m/s); (2) ice parcel velocity is less than the value in the previous time step; and (3) $\delta = |\dot{\varepsilon}_1 - \dot{\varepsilon}_2|$ is less than a small critical value $\delta_c = 1 \times 10^{-4}\ s^{-1}$. When these critical conditions are reached, the following approximation is introduced to calculate ice stresses for the ice parcel,

$$\sigma_{ij} = \sigma_{ijc} \frac{P}{P_c}, \tag{50}$$

in which σ_{ijc} and P_c are values of σ_{ij} and P corresponding to the above-mentioned critical conditions. In addition, when the velocity of an ice parcel remains less than 0.5 mm/s, the parcel is stopped. Using this method, ice jam formation can be simulated by the viscous-plastic constitutive law.

5. MODEL APPLICATION

Ice retention structures such as floating booms installed upstream of a river reach with high jamming potential could alleviate ice jam problems by preventing or reducing ice discharge to the problem reach. A floating ice boom is designed to submerge when the ice load becomes excessive, thereby allowing the ice to pass over the boom. In order for the boom to be effective additional hydraulic conditions have to be satisfied. The surface water velocity at the boom site has to be less than a critical entrainment velocity so that ice floes arriving at the site will not turn under at the boom or at the leading edge of the ice accumulated behind the boom. The flow velocity underneath the ice accumulation should also be less than a critical erosion velocity. Due to the highly unsteady nature of river ice processes, the use of laboratory models or field tests to determine the feasibility and design of ice booms can be costly and difficult. Numerical modeling provides a viable alternative for this purpose, as demonstrated in the following feasibility study for an ice boom in the Missouri River upstream of the Mississippi–Missouri River confluence.

The middle Mississippi River, which stretches 198 miles from its confluence with the Missouri River near St. Louis to where it joins the Ohio River at Cairo, Illinois, is a vital navigation route. During winter months, ice from the Missouri River and the ice generated in the uncontrolled sections of the Mississippi River can form accumulations that block off the middle Mississippi to shipping. Tuthill and Mamone [40] suggested the possibility of installing ice booms in the lower Missouri River to reduce the potential for ice jams in the middle Mississippi River. They examined the winter flow conditions in the Missouri River and suggested that river mile (RM) 16 is a possible location for an ice boom. A numerical study was performed using the present numerical model to study the feasibility of such an installation [20]. A simulation of the boom load resulting from an ice run, which caused an ice jam in the middle Mississippi River in January 1977, is presented in this section. The model domain covers the reach between RM 13 and RM 20 with the boom located at RM 16. The channel geometry is shown in Figs. 5 and 6.

The bed roughness was first calibrated based on the observed water level and discharge data for an open water condition that occurred in September 1994 and compared with the backwater simulation results of Tuthill and Mamone [40]. The ice model parameters were calibrated with the data of the January 1997 ice jam event. The calibrated model parameters are given in Table I. The initial condition was a steady state ice-free flow at a discharge of 566 m^3/s (20,000 cfs). The downstream boundary condition imposed at RM 13 was a water surface elevation of 123.6 m (405.6 ft). Upstream boundary conditions consisted of a constant water discharge of 566 m^3/s (20,000 cfs) and an ice discharge of 11.3 m^3/s (400 cfs). The goal of the simulation was to examine the development of ice

TABLE I
Parameters Used in the Ice Dynamic Simulation

Parameter	Description	Value
N_{max}	Maximum ice concentration	0.6
ϕ	Internal friction angle of ice	46°
$\tan\phi$	Boundary friction coefficient	1.04
j	Empirical constant	15
n_i	Manning's coefficient on ice	$0.02 \sim 0.06$

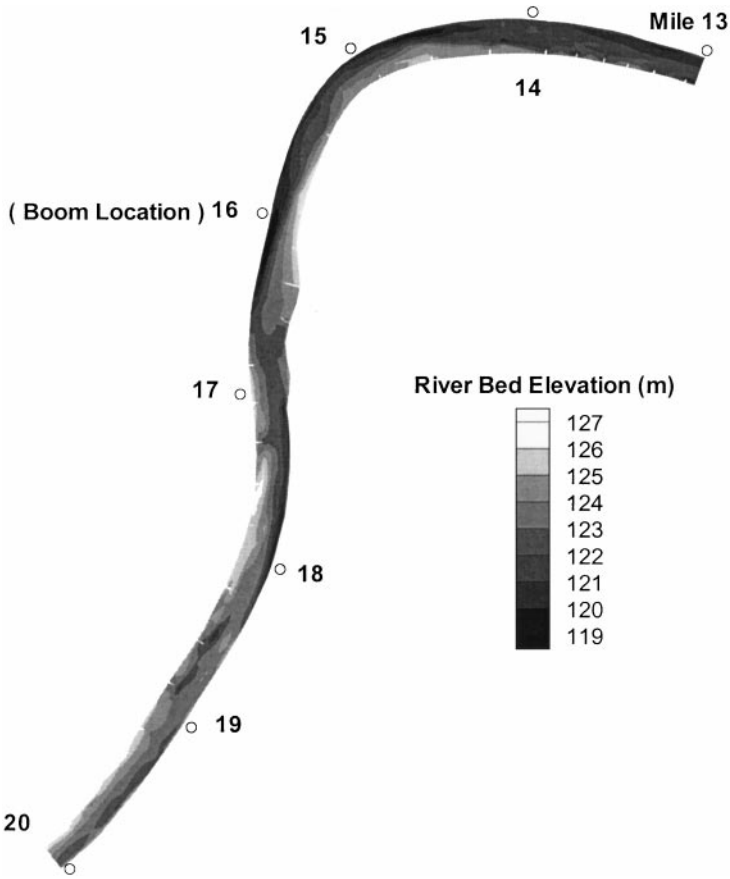

FIG. 5. Bed elevation between RM 13 and RM 20.

jam and boom load under a normal flow condition assuming that the boom was 100% effective. Limiting conditions for ice accumulation behind the boom were not imposed in the simulation. It was assumed that no ice entrainment or erosion would occur and that no ice would pass the boom. The simulation results indicated that the ice thickness at the boom location was large and that the ice grounded across most of the channel width near

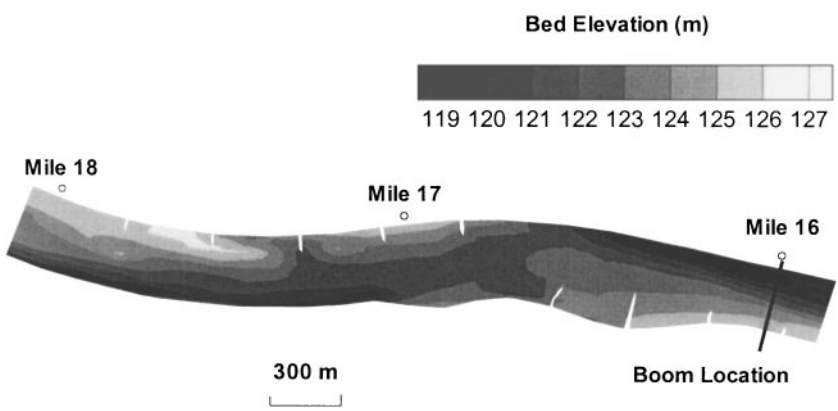

FIG. 6. Bed elevation in the vicinity of the boom.

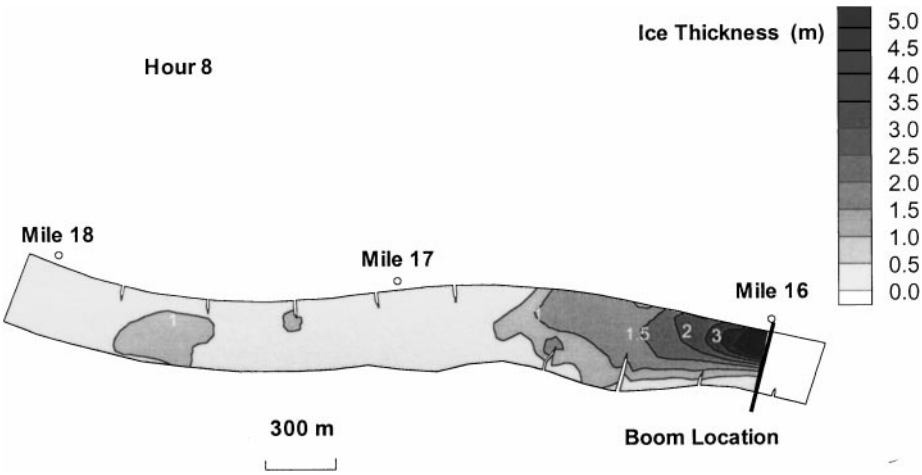

FIG. 7. Simulated ice thickness distribution behind the boom, $t = 8$ h.

the boom, as shown in Figs. 7–9. The ice accumulation increased upstream water levels significantly, as shown in Fig. 10. The load distribution on the boom is shown in Fig. 11. The boom load leveled off as the jam extended upstream. This was due to the grounding of the jam, as well as the increase in bank resistance as the jam progressed upstream. The maximum load per unit width was in the range of 40 to 50 kN/m, which was too high for a conventional river ice boom. Before the present study, ice retention behind booms was considered to be marginally possible, based on a conventional one-dimensional static ice jam model [40]. For problem ice years on the middle Mississippi River, average Missouri River discharge is about 850 m^3/s (30,000 cfs). Numerical simulations carried out in the present study found that ice retention behind booms is unfeasible even at a much lower discharge of 566 m^3/s (20,000 cfs). Additional simulations also showed that under-ice water velocities near booms were sufficiently high to cause ice erosion and to halt upstream ice cover progression. Ice retention behind booms is not feasible in this reach, unless a specially designed boom with high retention capacity can be developed.

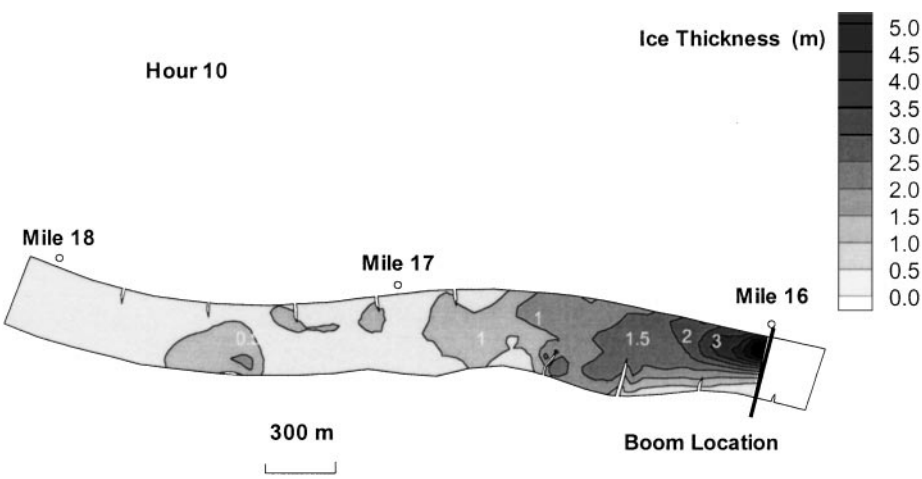

FIG. 8. Simulated ice thickness distribution behind the boom, $t = 10$ h.

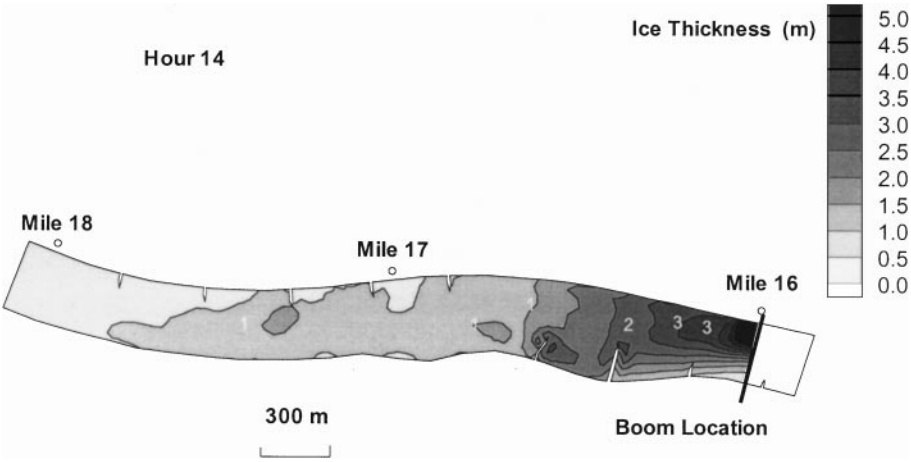

FIG. 9. Simulated ice thickness distribution behind the boom, $t = 14$ h.

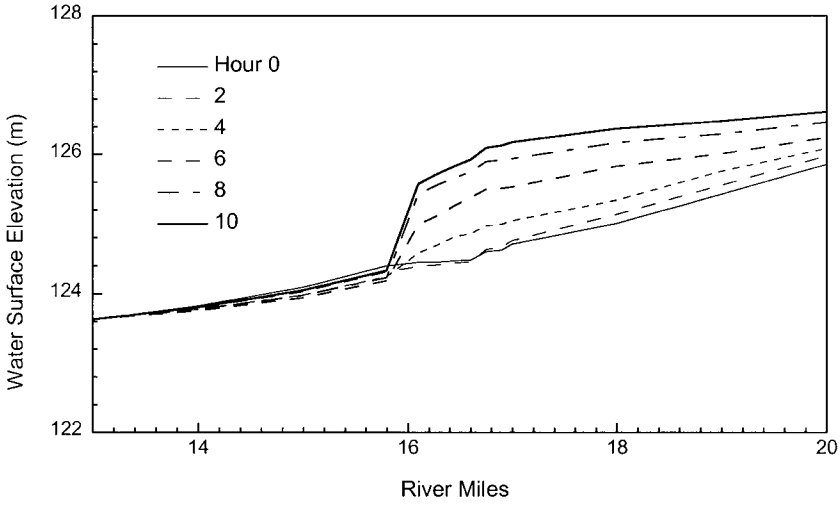

FIG. 10. Simulated water surface profiles.

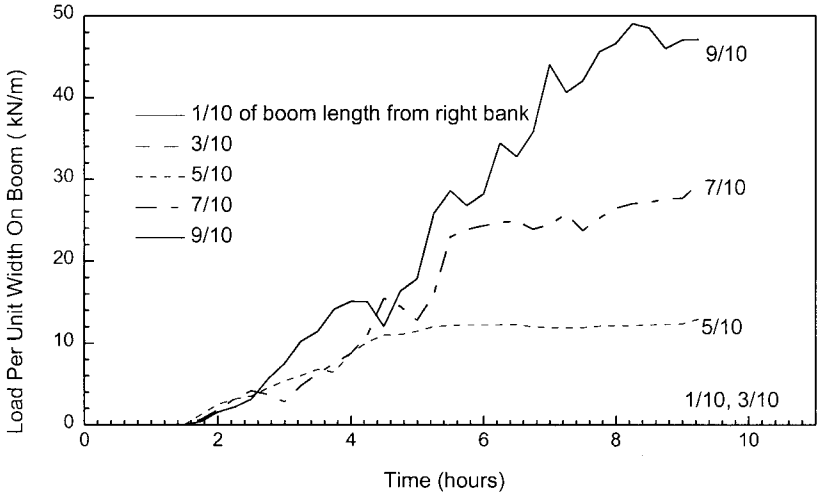

FIG. 11. Simulated boom load variations across the channel.

6. SUMMARY AND CONCLUSION

A two-dimensional numerical model for dynamic transport and jamming of surface ice in rivers is presented. The hydrodynamic component of the model uses an Eulerian finite-element method, while the ice dynamic component of the model uses the Lagrangian smoothed-particle hydrodynamics method. The model considers the moving surface ice as a continuum. The internal ice resistance is formulated according to a viscous–plastic constitutive law, in which the pressure term is formulated by modifying the coulomb-type constitutive relationship for static ice jams. The partial-slip dynamic boundary condition for ice along river banks and other solid boundaries is treated by the method of images. Ice entrainment at floating ice booms or the leading edge of the ice accumulation, erosion of ice on the underside of the ice accumulation, and the limiting ice boom load for ice retention were considered in the model.

The numerical model was validated with analytical solutions for idealized static ice jams with or without bank friction. The model was used to study the feasibility of using ice booms to retain ice in the lower Missouri River to reduce the ice discharge into the Mississippi River. A conventional one-dimensional ice jam model predicted that stable ice accumulation was possible [40], but was unable to address the dynamic processes as well as ice erosion and entrainment. The present two-dimensional ice dynamic model proved to be a valuable tool for addressing important design issues that could not be answered by conventional methods. The model was able to determine if ice retention behind a proposed boom was possible. It could also determine the load distribution along the boom and answer the important question of whether the accumulation behind the boom would be able to progress upstream. In addition to its application in ice boom designs, the numerical model is capable of simulating dynamic ice transport and jamming processes in natural rivers with complex geometry and flow conditions [21].

ACKNOWLEDGMENT

This work was partially supported by the U.S. Army Research Office under Contract DACA89-94-K0017.

REFERENCES

1. J. Bear, *Dynamics of Fluids in Porous Media* (Elsevier, New York, 1972).
2. S. Beltaos, Numerical computation of river ice jams, *Can. J. Civil Eng.* **20**(1), 88 (1993).
3. S. Beltaos, Ed., *River Ice Jams* (Water Resources Publications, Highland Ranch, CO, 1995).
4. W. Benz, Smooth particle hydrodynamics, in *The Numerical Modeling of Nonlinear Stellar Pulsations*, edited by J. R. Bucher (Kluwer Academic, Dordrecht, 1990), p. 269.
5. J. J. Connor and C. A. Brebbia, *Finite Element Techniques for Fluid Flow* (Butterworth, Stoneham, MA, 1978).
6. A. E. Evrard, Beyond N-body: 3D cosmological gas dynamics, *Mon. Not. R. Astron. Soc.* **235**, 911 (1988).
7. G. Flato, A particle-in-cell sea-ice model, *Atmos. Ocean* **31**(3), 339 (1993).
8. G. Flato and R. Gerard, Calculation of ice jam thickness profile, *J. Hydraul. Res.* **28**(6), 737 (1986).
9. R. A. Gingold and J. J. Monaghan, Smoothed particle hydrodynamics: Theory and application to non-spherical stars, *Mon. Not. R. Astron. Soc.* **181**, 375 (1977).
10. R. A. Gingold and J. J. Monaghan, Kernel estimates as a basis for general particle method in hydrodynamics, *J. Comput. Phys.* **46**, 429 (1982).
11. J. Goodman and L. Hernquist, Hydrodynamics of collision between binary stars, *Astrophys. J.* **37**, 637 (1991).

12. D. M. Hanes and D. L. Inman, Experimental evaluation of a dynamic yield criterion for granular fluid flows, *J. Geophys. Res. B* **90**(5), 3670 (1985).
13. F. H. Harlow, The particle-in-cell computing method for fluid dynamics, *Methods Comput. Phys.* **3**, 319 (1964).
14. P. Helman, R. Veroff, and F. R. Carrano, *Intermediate Problem Solving and Data Structure* (Benjamin–Cummings, Redwood City, CA, 1991).
15. L. Hernquist and N. Katz, TREESPH: A unification of SPH with the hierarchical tree method, *Astron. J. Supp. Ser*. **70**, 419 (1989).
16. W. D. Hibler, III, A dynamic thermodynamic sea ice model, *J. Phys. Oceanogr.* **9**, 815 (1979).
17. R. W. Hockyney and J. W. Eastwood, *Computer Simulation Using Particles* (McGraw–Hill, New York, 1981).
18. A. M. W. Lal and H. T. Shen, Numerical simulation of river ice dynamics, in *Proceedings of the 3rd International Conference on Ice Technology, Cambridge, MA, 1992*.
19. L. D. Libersky and A. G. Petschek, Smooth particle hydrodynamics with strength of materials, in *Advances in the Free-Lagrange Method*, edited by H. E. Trease, M. J. Frittes, and W. P. Crowley, Lecture Notes in Physics (Springer-Verlag, Berlin, 1991), Vol. 395, pp. 248.
20. L. W. Liu and H. T. Shen, *Numerical Simulation of River Ice Control with Booms*, CRREL Report No. 672 (U.S. Army Cold Regions Research and Engineering Lab., Hanover, NH, 1999).
21. L. W. Liu, H. T. Shen, and A. M. Tuthill, A numerical model for river ice jam evolution, in *Ice in Surface Waters*, edited by H. T. Shen (Balkema, Rotterdam, 1999), p. 739.
22. L. B. Lucy, A numerical approach to the testing of the fission hypothesis, *Astron. J.* **82**, 1013 (1977).
23. R. W. MacCormack, *A Numerical Method for Solving the Equations of Compressible Viscous Flow*, AIAA Paper 81-0110 (AIAA, 1981).
24. C. S. McCormick and T. F. Miller, Simulation of shock-wave reflection in a one-dimensional shock tube using smoothed particle hydrodynamics, *Numer. Heat Transfer B* **26**, 473 (1994).
25. J. J. Monaghan, Why particle methods work, *SIAM J. Sci. Stat. Comput.* **3**(4), 22 (1982).
26. J. J. Monaghan, Particle methods for hydrodynamics, *Comput. Phys. Rep.* **3**, 71 (1985).
27. J. J. Monaghan, On the problem of penetration in particle method, *J. Comput. Phys.* **82**, 1 (1989).
28. J. J. Monaghan, Smoothed particle hydrodynamics, *Annu. Rev. Astron. Astrophys.* **30**, 543 (1992).
29. J. J. Monaghan, Simulating free surface flows with SPH, *J. Comput. Phys.* **110**, 399 (1994).
30. J. J. Monaghan and A. Kocharyan, SPH simulation of multi-phase flow, *Comput. Phys. Commun.* **87**, 225 (1995).
31. J. P. Morris and J. J. Monaghan, A switch to reduce SPH viscosity, *J. Comput. Phys.* **136**, 41 (1997).
32. R. Pariset and H. Hausser, Formation and evolution of ice covers on rivers, *ASME EIC Hydrauliscs Conf. 61-EIC-6, Trans. Eng. Inst. Canada* **5**(1), 41 (1961).
33. R. S. Pritchard, A. C. Muller, D. J. Hanzlick, and Y. S. Yang, Forecasting Bering Sea ice edge behavior, *J. Geophys. Res. C* **95**(1), 775 (1990).
34. F. A. Rasio and S. L. Shapiro, Collisions of giant stars with compact objects: Hydrodynamic calculations, *Astron. J.* **377**, 559 (1991).
35. C. E. Rhoades, Jr., A fast algorithm for calculating particle interactions in smooth particle hydrodynamic simulations, *Comput. Phys. Commun.* **70**, 478 (1992).
36. H. T. Shen and Y. C. Chen, *Lagrangian Discrete Parcel Simulation of Two-Dimensional River Ice Dynamics*, Report 92-9 (Department of Civil and Environ. Engrg., Clarkson University, Potsdam, NY, 1992).
37. H. T. Shen, Y. C. Chen, A. Wake, and R. D. Crissman, Lagrangian discrete parcel simulation of two-dimensional river ice dynamics, *Int. J. Offshore Polar Eng.* **3**, 328 (1993).
38. H. T. Shen, H. H. Shen, and S. M. Tsai, Dynamic transport of river ice, *J. Hydraul. Res.* **28**, 659 (1990).
39. J. W. Swegle, D. L. Hicks, and S. W. Attaway, Smoothed particle hydrodynamics stability analysis, *J. Comput. Phys.* **116**, 123 (1995).
40. A. M. Tuthill and A. C. Mamone, Structural ice control alternatives for middle Mississippi River, *ASCE J. Cold Regions Eng.* **12**, 202 (1998).
41. A. Wake and R. R. Rumer, Great Lakes ice dynamics simulation, *J. Waterway Port Coast. Ocean Eng.* **109**, 86 (1983).